Possible production of neutron-rich Md isotopes in multinucleon transfer reactions with Cf and Es targets

Myeong-Hwan Mun,[1,2] Kyujin Kwak,[2,*] G. G. Adamian,[3] and N. V. Antonenko[3,4]
[1]*Korea Institute of Science and Technology Information, Daejeon, 34141, Korea*
[2]*Ulsan National Institute of Science and Technology, Ulsan, 44919, Korea*
[3]*Joint Institute for Nuclear Research, 141980 Dubna, Russia*
[4]*Mathematical Physics Department, Tomsk Polytechnic University, 634050 Tomsk, Russia*

(Received 13 January 2019; revised manuscript received 23 April 2019; published 30 May 2019)

The possibilities for production of yet unknown neutron-rich isotopes $^{261–265}$Md are explored in the multinucleon transfer reactions with stable beams bombarding on Cf and Es targets. The production of a given isotope of neutron-rich Md is optimized by appropriate choices of projectile-target combinations and bombarding energies. The production cross sections of neutron-rich Md isotopes in the $0n$ and $1n$ evaporation channels of multinucleon transfer reactions are compared. The prospects for the use of radioactive beams in the production of new Md isotopes are discussed.

DOI: 10.1103/PhysRevC.99.054627

I. INTRODUCTION

The complete fusion and fragmentation reactions cannot be used to produce new neutron-rich transactinides because of the lack of proper projectile-target combinations. For example, in order to produce neutron-rich Md isotopes in the complete fusion reactions with the ^{30}Si and ^{48}Ca beams, very short-lived (less than a few minutes) isotopes of Fr and Tl are required to be used for targets, which is impossible at the moment. While the complete fusion and fragmentation reactions fail, the multinucleon transfer reactions are the only way to produce new neutron-rich isotopes of actinides and transactinides. For instance, one can use ^{254}Es (half-life is about 276 days) or $^{249–252}$Cf targets for the production of new neutron-rich Md isotopes in the transfer reactions with stable beams. The radioactive neutron-rich beams with the high intensity can be employed further to produce new neutron-rich isotopes in the transfer reactions. So, the transfer reactions provide us with an efficient tool with which we can explore the region of unknown isotopes of heaviest nuclei.

The multinucleon transfer reactions have been known to be effective for producing exotic nuclei for many years [1–34]. The transfer products accompany the complete fusion reactions [18,21,22,24,25]. In Refs. [35,36], the possibility has been shown to produce isotopes close to the neutron drip line in the transfer reactions at incident energies close to the Coulomb barrier. In Refs. [37,38], a model was suggested to predict the optimal projectile-target combinations as well as bombarding energies and estimate the production cross sections. Finding a global trend in the production cross section of exotic nuclei in the multinucleon transfer reactions with suitable theoretical calculations helps to increase the efficiency of experiments that produce exotic nuclei. Based on the trend found, one can select the best candidates for the optimal beam-target combination which have large cross sections. Because the production cross sections of some unknown neutron-rich isotopes are estimated to be very small, it is important to predict their production cross sections as accurately as possible before the future experiments to produce them are designed and performed.

In Ref. [39], we studied the production of Md isotopes in the transfer reactions ^{48}Ca + ^{238}U, ^{242,244}Pu, and ^{245,246,248}Cm. The largest yield of neutron-rich isotopes was predicted in the ^{48}Ca + ^{244}Pu reaction. To complete this study, in the present paper, we consider the production of Md isotopes in the transfer reactions on the Cf and Es targets which can be available in the future experiments. Besides the reactions with the ^{48}Ca beam, we also consider reactions with neutron-rich light nuclei like ^{14}C and ^{18}O. In addition to the production of Md isotopes in the $0n$ evaporation channel, the $1n$ evaporation channel is also considered to show the dependence of isotopic yields on bombarding energy. Though the model is described in detail in Refs. [37–39], we shortly present its main points in Sec. II. The results of our calculations are given in Sec. III. We summarize our results in Sec. IV.

II. ISOTOPIC YIELDS IN TRANSFER REACTIONS

The dinuclear system (DNS) model describes the evolution of the interacting nuclei along three collective degrees of freedom: the relative distance R between the center of the nuclei and the charge and mass (neutron) asymmetry coordinates' degrees of freedom, which are defined here by the charge Z and neutron N numbers of a heavy nucleus of the

*kkwak@unist.ac.kr

DNS. After the dissipation of kinetic energy and angular momentum of the relative motion, the entrance channel (initial) DNS with the nucleus $(Z^{(i)}, N^{(i)})$, the definite total charge number $Z_{\rm tot}$, mass number $A_{\rm tot}$, and the average excitation energy and angular momentum is formed at the touching distance between the nuclei $R = R_m$. Then, the nucleon drift and nucleon diffusion occur between the DNS nuclei, which leads to the formation of various DNS configurations and compound nucleus. The excited DNS with some Z and N can decay into two fragments by the diffusion which are in relative distance R between the centers of the DNS nuclei. These decays result in the primary yield of reaction products. Then, the primary fragments are mainly de-excited by neutron and γ emission or go to fission channel.

So, in our approach, the production of a certain nucleus is made through a three-step process. First, the initial DNS with the nucleus $(Z^{(i)}, N^{(i)})$ is formed in the entrance reaction channel. Second, the DNS with exotic nucleus (Z, N) is created through nucleon transfers. Finally, this DNS is divided into two fragments. The created exotic neutron-rich nuclei (Z, N) are de-excited. The production cross section of nucleus with charge Z and neutron $N - x$ numbers is calculated as follows:

$$\sigma_{Z,N-x} = \sigma_{\rm cap} Y_{Z,N} W_{\rm sur}^{xn}, \tag{1}$$

where $\sigma_{\rm cap}$, $Y_{Z,N}$, and $W_{\rm sur}^{xn}$ are the capture cross section, the formation-decay probability of the DNS configuration with the given charge and mass asymmetries, and the survival probability of the excited exotic neutron-rich nucleus (Z, N) in the xn ($x = 0, 1, 2, ...$ is the number of the emitted neutrons) evaporation channel, respectively. At the bombarding energy $E_{\rm c.m.}$ above the Coulomb barrier, the capture cross section is expressed as

$$\sigma_{\rm cap} = \frac{\pi\hbar^2}{2\mu E_{\rm c.m.}} J_{\rm cap}(J_{\rm cap} + 1), \tag{2}$$

where μ is the reduced mass of the projectile-target system. The value of angular momentum $J_{\rm cap}$ is determined by the bombarding energy. If the value of $E_{\rm c.m.}$ is close to the Coulomb barrier energy, $J_{\rm cap}$ does not exceed 30–40. However, the angular momentum decreases the stability of the exotic nuclei of interest. So, we choose $J_{\rm cap} = 30$ to produce neutron-rich isotopes of interest with rather small angular momenta.

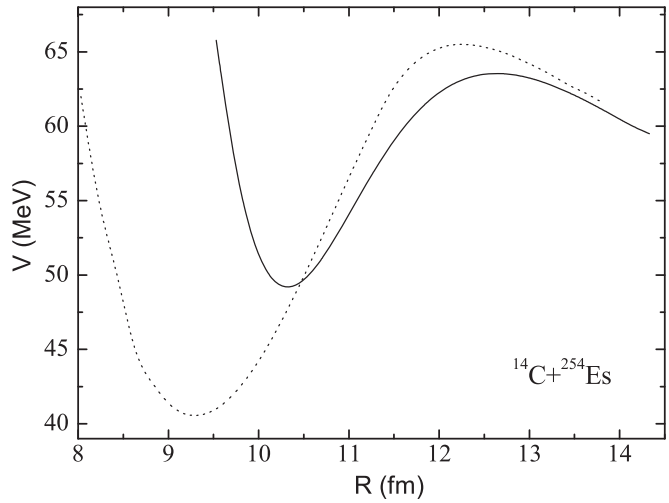

FIG. 1. The comparison of nucleus-nucleus potential used in the calculations (solid line) with the proximity potential [44] for the $^{14}\mathrm{C} + {}^{254}\mathrm{Es}$ reaction. The interacting nuclei are assumed to be spherical.

To calculate the value of $Y_{Z,N}$ with the statistical method, the DNS potential energy is used as in Refs. [37,40–43]:

$$U(R, Z, N, J) = B_1 + B_2 + V(R, Z, N, J), \tag{3}$$

where B_1 and B_2 are the mass excesses of the light and heavy nucleus, respectively. The nucleus-nucleus interaction potential V between two nuclei includes the Coulomb interaction, the nuclear interaction, and the centrifugal term. We refer the details for the calculation of the potential V to Refs. [37,43]. In Fig. 1, we compare the nucleus-nucleus potential $V(R)$ used with the proximity potential [44] for the $^{14}\mathrm{C} + {}^{254}\mathrm{Es}$ reaction. The nuclei are assumed to be spherical because the effect of deformation is almost the same in any method of the calculation of $V(R)$. The proximity potential results in the Coulomb barrier of a few MeV higher. The position of this barrier is shifted by about 0.5 fm to smaller R with respect to that $V(R)$ used in our calculations. The double-folding procedure used in Refs. [37,43] does not allow nuclei to overlap as much as the proximity potential. So, with V used, the overlap of interacting nuclei is relatively small to consider the nucleon exchange in the DNS.

The formation-decay probability is calculated with the expression introduced in Refs. [35,36], which reads

$$Y_{Z,N} \approx 0.5 \exp\left[-\frac{U(R_m(Z, N_0), Z, N_0, J) - U(R_m(Z^{(i)}, N^{(i)}), Z^{(i)}, N^{(i)}, J) - B_{\rm qf}(Z^{(i)}, N^{(i)})}{\Theta(Z^{(i)}, N^{(i)})} - \frac{B_R(Z, N)}{\Theta(Z, N_0)}\right]. \tag{4}$$

Here, we use the DNS potential energy U at the touching distance $R_m(Z, N) \approx R_{01}(1 + \sqrt{5/(4\pi)}\beta_2^{(1)}) + R_{02}(1 + \sqrt{5/(4\pi)}\beta_2^{(2)}) + 0.5$ fm, where $R_{0i} = 1.15A_i^{1/3}$ fm is the mass radius of each nucleus with mass number A_i in the DNS and $\beta_2^{(1)}$ and $\beta_2^{(2)}$ are the parameters of quadrupole deformation of the DNS nuclei. The decaying DNS with given Z and N can escape from the local minimum at $R = R_m(Z, N)$ by overcoming the potential barrier at $R = R_b(Z, N)$, where $R_b(Z, N) \approx R_m(Z, N) + 2$ fm. The height of the barrier which the DNS with Z and N_0 should overcome in order to produce a nucleus with Z and N as a primary product is given by $B_R^{\rm qf}(Z, N) = U(R_b(Z, N), Z, N, J) - U(R_m(Z, N_0), Z, N_0, J)$. Note that the neutron number N_0 in the DNS is determined by the N/Z

equilibrium in the DNS at given Z, i.e., the conditional minimum of the potential energy surface. In Eq. (4), the term of $B_{\rm qf} = \min(B_\eta^{\rm asym}, B_\eta^{\rm sym}, B_R^{\rm qf})$ is the barrier that plays a role of preventing the DNS from decaying either in R or toward more asymmetric-symmetric configurations. The values of $B_\eta^{\rm sym}$ and $B_\eta^{\rm asym}$ measure the barriers for the initial DNS toward more symmetric and asymmetric configurations, respectively. For example, more asymmetric configurations should be taken into account if we consider the strongly asymmetric transfer reactions like with the projectiles C and O.

In Eq. (4), the temperature $\Theta(Z^{(i)}, N^{(i)})$ is estimated using the Fermi-gas expression $\Theta = \sqrt{E^*/a}$ with the excitation energy $E^*(Z^{(i)}, N^{(i)})$ of the initial DNS and with the level-density parameter $a = A_{\rm tot}/12$ MeV^{-1}. The temperature $\Theta(Z, N_0)$ is calculated for the excitation energy $E^*(Z^{(i)}, N^{(i)}) - [U(R_m(Z, N_0), Z, N_0, J) - U(R_m(Z^{(i)}, N^{(i)}), Z^{(i)}, N^{(i)}, J)]$.

In the excited DNS that formed from the initial DNS by diffusive nucleon transfers and contains neutron-rich nucleus, one can assume thermal equilibrium and thus define the excitation energy of the light or heavy nucleus with mass number A_1 or A_2 as follows:

$$E^*_{1,2}(Z, N) = \frac{A_{1,2}}{A_{\rm tot}}\Big[E^*(Z^{(i)}, N^{(i)}) - B_R^{qf}(Z, N)\Big]. \quad (5)$$

The deviation from thermal equilibrium is expected only for the DNS near the initial DNS with $(Z^{(i)}, N^{(i)})$ which formed almost instantaneously. If one nucleus in the DNS is magic, it has a smaller excitation energy than that determined by Eq. (5). So, our estimates of production cross sections with Eq. (5) correspond to the upper limits of the yields. The cross section $\sigma_{Z,N}$ for the production of neutron-rich nucleus with (Z, N) increases with $E^*(Z^{(i)}, N^{(i)})$ until $E^*_1(Z, N)$ or $E^*_2(Z, N)$ is equal to neutron separation energy $S_n(Z, N)$ or fission barrier $B_f(Z, N)$ if $B_f(Z, N) < S_n(Z, N)$. Up to this point, $W^{0n}_{\rm sur} = 1$ and the primary and secondary yields coincide. A further increase of $E^*_{1,2}(Z, N)$ would increase (decrease) the primary (secondary) yield.

At the excitation energy exceeding S_n and B_f, the primary excited neutron-rich nucleus either emits neutrons or goes to fission. In the case that the primary nucleus emits neutron, it contributes to the yield of secondary nucleus that has a smaller number of neutrons. The competition between neutron evaporation and fission is taken into account with the factor

$$W^{1n}_{\rm sur} = P_{1n}\frac{\Gamma_n}{\Gamma_n + \Gamma_f}, \quad (6)$$

where P_{1n} is the probability of realization of the $1n$ evaporation channel at given excitation energy, and Γ_n and Γ_f are the widths of neutron evaporation and fission, respectively. These values are calculated as in Ref. [45]. To obtain a maximal value of W_{1n}, the excitation energy $E^*(Z, N)$ should correspond to the maximum of $P_{1n} \approx 1$. So, in the calculation of production cross sections of the isotopes in the $1n$ evaporation channel, we choose the bombarding energy in accordance with this condition. In calculations, the mass excesses and, correspondingly, the neutron separation energies S_n as well as the fission barriers for unknown nuclei are taken from the predictions of the finite-range liquid-drop model presented in Ref. [46]. As shown in Ref. [47], the WS4 model [48] provides the best average agreement with the experimental nuclear masses. However, for $^{258-264}$Md, the predicted values of S_n are almost the same in Refs. [46,48]. The predicted values of B_f are only available in Ref. [46] and used in our calculations. The mass excesses differ within 1 MeV in the models mentioned. If we use the predicted masses from Ref. [48], the maximum cross sections in $0n$ channel are shifted up in $E_{\rm c.m.}$ within 1 MeV.

To test the method of calculation, we compare compare the results obtained for some reactions with available experimental data. In the ^{86}Kr + ^{104}Ru reaction at $E_{\rm c.m.} = 178.6$ MeV, the Zr isotopes are produced with excitation energies which do not allow neutron evaporation. So, the calculated primary yields 0.4, 0.07, 0.06, and 0.004 mb for $^{95-98}$Zr, respectively, can be compared with the experimental data. For ^{95,97}Zr, the measured cross sections [27] are 1 ± 0.2 and 0.11 ± 0.02 mb, respectively, which is consistent with our calculations. The isotopes of Mo are produced in this reaction with excitations at which $1n$ emission occurs because the DNS with Mo are more deformed than those with Zr and their deformation energies are transformed into the excitations of the products. The calculated yields 0.3, 2.2, 0.74, and 2.87 mb for $^{98-101}$Mo, respectively, are in satisfactory agreement with the experimental data 2.35 ± 0.25 and 1.6 ± 0.3 mb for ^{99,101}Mo, respectively.

As another example, we consider the production of ^{12,13,14}C in the reactions ^{16,18}O + ^{90}Zr. For the ^{16}O + ^{90}Zr ($E_{\rm c.m.} = 76$ MeV) reaction, our calculated cross sections are 20, 3, and 3.4 mb for ^{12,13,14}C, respectively, while the

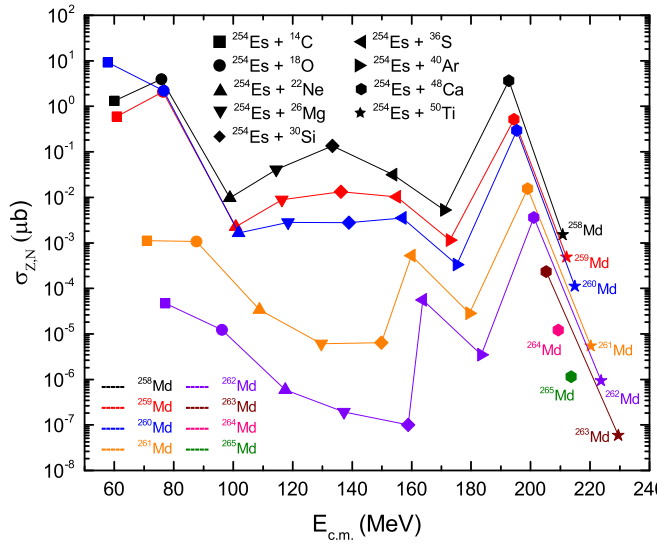

FIG. 2. The expected maximal production cross sections of neutron-rich isotopes $^{258-265}$Md in the $0n$ evaporation channel of the indicated multinucleon transfer reactions ^{14}C + ^{254}Es (squares), ^{18}O + ^{254}Es (circles), ^{22}Ne + ^{254}Es (triangles), ^{26}Mg + ^{254}Es (inverted triangles), ^{30}Si + ^{254}Es (rhombuses), ^{36}S + ^{254}Es (left-pointing triangles), ^{40}Ar + ^{254}Es (right-pointing triangles), ^{48}Ca + ^{254}Es (hexagons), and ^{50}Ti + ^{254}Es (stars). The lines trace the results for the same isotopes of Md. The lines with different colors correspond to different isotopes of Md.

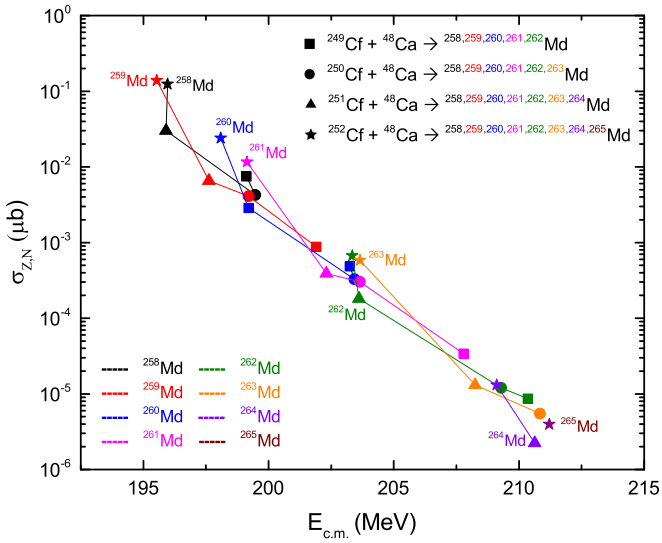

FIG. 3. The expected maximal production cross sections of neutron-rich isotopes $^{258–265}$Md in the $0n$ evaporation channel of the indicated multinucleon transfer reactions ^{48}Ca + ^{249}Cf (squares), ^{48}Ca + ^{250}Cf (circles), ^{48}Ca + ^{251}Cf (triangles), and ^{48}Ca + ^{252}Cf (stars). The lines trace the results for the same isotopes of Md. The lines with different colors correspond to different isotopes of Md.

experimental cross sections are 60, 20, and 18 mb [29]. In the ^{18}O + ^{90}Zr ($E_{c.m.}$ = 75 MeV) reaction, the calculated cross sections 17, 34, and 5.6 mb for ^{12,13,14}C, respectively, are also consistent with the experimental ones of 10, 8, and 12 mb. As seen, our model can reproduce the existing experimental data with satisfactory accuracy, up to the factor of 3.

III. CALCULATED RESULTS

The calculated production cross sections are presented in Fig. 2 for neutron-rich isotopes $^{258–265}$Md in the $0n$ evaporation channel of multinucleon transfer reactions

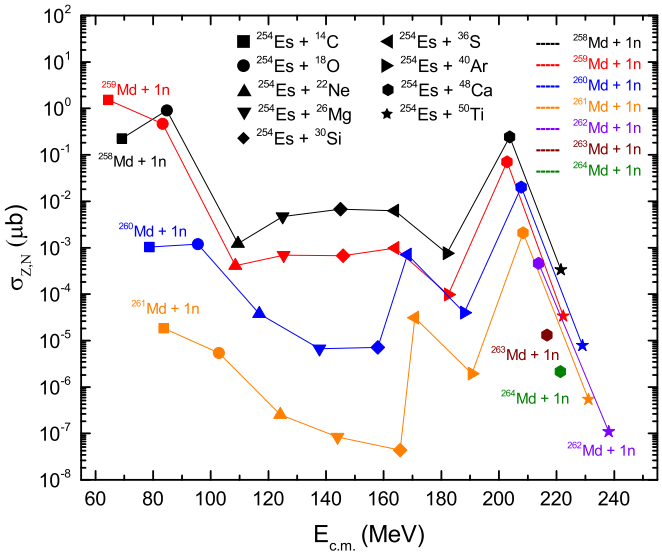

FIG. 4. The same as in Fig. 2, but for the $1n$ evaporation channel.

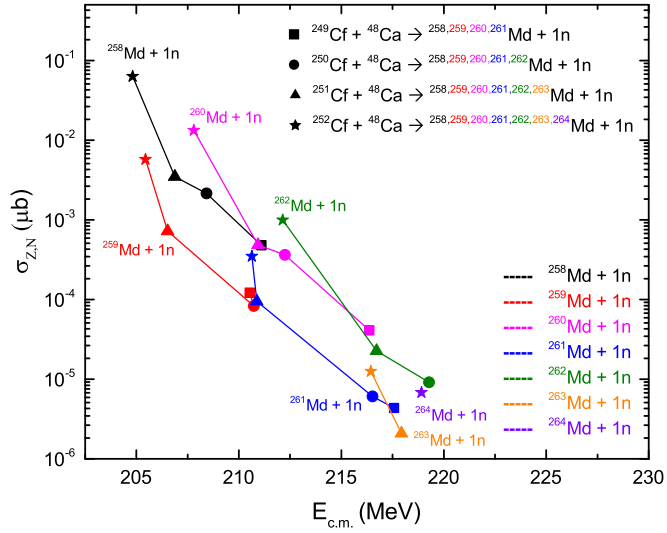

FIG. 5. The same as in Fig. 3, but for the $1n$ evaporation channel.

^{14}C, ^{18}O, ^{22}Ne, ^{26}Mg, ^{30}Si, ^{36}S, ^{40}Ar, ^{48}Ca, and ^{50}Ti + ^{254}Es. In these reactions, the nuclei of interest are produced in accordance with the following three-step schemes: ^{14}C + ^{254}Es → ^{14}C + ^{254}Es → $^{10–6}$Be + $^{258–262}$Md, ^{18}O + ^{254}Es → ^{22}O + ^{250}Es → $^{14–10}$C + $^{258–262}$Md, ^{22}Ne + ^{254}Es → ^{24}Ne + ^{252}Es → $^{18–14}$O + $^{258–262}$Md, ^{26}Mg + ^{254}Es → ^{28}Mg + ^{252}Es → $^{22–18}$Ne + $^{258–262}$Md, ^{30}Si + ^{254}Es → ^{34}Si + ^{250}Es → $^{26–22}$Mg + $^{258–262}$Md, ^{36}S + ^{254}Es → ^{40}S + ^{250}Es → $^{32–28}$Si + $^{258–262}$Md, ^{40}Ar + ^{254}Es → ^{46}Ar +

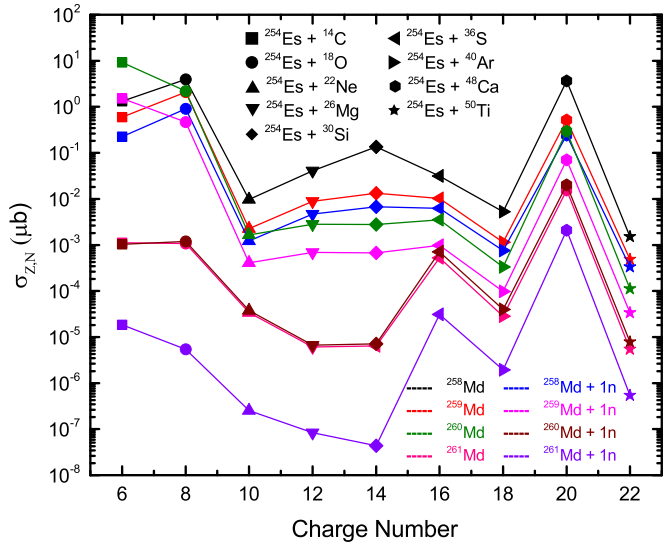

FIG. 6. The expected maximal production cross sections of neutron-rich isotopes $^{258–261}$Md as a function of atomic number of the projectile in the $0n$ and $1n$ evaporation channels of the indicated multinucleon transfer reactions ^{14}C + ^{254}Es (squares), ^{18}O + ^{254}Es (circles), ^{22}Ne + ^{254}Es (triangles), ^{26}Mg + ^{254}Es (inverted triangles), ^{30}Si + ^{254}Es (rhombuses), ^{36}S + ^{254}Es (left-pointing triangles), ^{40}Ar + ^{254}Es (right-pointing triangles), ^{48}Ca + ^{254}Es (hexagon), and ^{50}Ti + ^{254}Es (stars). The lines with different colors correspond to different isotopes of Md produced with different channels.

TABLE I. The predicted cross sections $\sigma_{Z,N}$ of the production of neutron-rich isotopes ^{258,259,260,261}Md in the transfer reactions ^{254}Es + ^{14}C, ^{18}O, ^{22}Ne, ^{26}Mg, ^{30}Si, ^{36}S, ^{40}Ar, ^{48}Ca, and ^{50}Ti. The optimal bombarding energies $E_{\text{c.m.}}$, capture cross sections σ_{cap}, and formation-decay probabilities $Y_{Z,N}$ are listed. For the 1n evaporation channel, the values of survival probability W_{1n} are presented.

Reactions	Isotopes	$E_{\text{c.m.}}$ (MeV)	σ_{cap} (b)	$Y_{Z,N}$	W_{1n}	$\sigma_{Z,N}$ (b)
	^{258}Md	60.08	0.76	1.74×10^{-6}		1.32×10^{-6}
	^{258}Md + 1n	69.10	0.66	8.14×10^{-6}	0.042	2.26×10^{-7}
	^{259}Md	60.81	0.75	7.95×10^{-7}		5.97×10^{-7}
^{14}C + ^{254}Es	^{259}Md + 1n	64.38	0.71	7.04×10^{-5}	0.031	1.53×10^{-6}
	^{260}Md	57.81	0.79	1.17×10^{-5}		9.26×10^{-6}
	^{260}Md + 1n	78.72	0.58	1.64×10^{-8}	0.109	1.03×10^{-9}
	^{261}Md	70.97	0.64	1.74×10^{-9}		1.12×10^{-9}
	^{261}Md + 1n	83.61	0.55	5.26×10^{-10}	0.064	1.84×10^{-11}
	^{258}Md	75.86	0.47	8.36×10^{-6}		3.97×10^{-6}
	^{258}Md + 1n	84.71	0.43	5.03×10^{-6}	0.042	9.00×10^{-7}
	^{259}Md	76.30	0.47	4.42×10^{-6}		2.09×10^{-6}
^{18}O + ^{254}Es	^{259}Md + 1n	83.26	0.43	3.51×10^{-5}	0.031	4.67×10^{-7}
	^{260}Md	76.59	0.47	4.70×10^{-6}		2.21×10^{-6}
	^{260}Md + 1n	95.47	0.38	2.89×10^{-8}	0.1089	1.19×10^{-9}
	^{261}Md	87.61	0.41	2.61×10^{-9}		1.07×10^{-9}
	^{261}Md + 1n	102.77	0.35	2.42×10^{-10}	0.064	5.42×10^{-12}
	^{258}Md	98.90	0.30	3.23×10^{-8}		9.78×10^{-9}
	^{258}Md + 1n	109.41	0.27	1.06×10^{-7}	0.042	1.22×10^{-9}
	^{259}Md	100.87	0.30	7.65×10^{-9}		2.27×10^{-9}
^{22}Ne + ^{254}Es	^{259}Md + 1n	108.54	0.29	4.82×10^{-8}	0.031	4.09×10^{-10}
	^{260}Md	101.77	0.29	5.65×10^{-9}		1.66×10^{-9}
	^{260}Md + 1n	116.80	0.26	1.36×10^{-9}	0.109	3.79×10^{-11}
	^{261}Md	108.83	0.27	1.24×10^{-10}		3.42×10^{-11}
	^{261}Md + 1n	124.16	0.24	1.65×10^{-11}	0.064	2.54×10^{-13}
	^{258}Md	114.46	0.22	1.82×10^{-7}		4.07×10^{-8}
	^{258}Md + 1n	124.99	0.21	5.44×10^{-7}	0.042	4.70×10^{-9}
	^{259}Md	116.32	0.22	4.01×10^{-8}		8.84×10^{-9}
^{26}Mg + ^{254}Es	^{259}Md + 1n	125.34	0.20	1.10×10^{-7}	0.031	6.93×10^{-10}
	^{260}Md	118.47	0.22	1.29×10^{-8}		2.80×10^{-9}
	^{260}Md + 1n	137.72	0.19	3.28×10^{-10}	0.109	6.66×10^{-12}
	^{261}Md	129.63	0.20	3.06×10^{-11}		6.06×10^{-12}
	^{261}Md + 1n	144.02	0.18	7.29×10^{-12}	0.064	8.32×10^{-14}
	^{258}Md	133.39	0.17	8.01×10^{-7}		1.35×10^{-7}
	^{258}Md + 1n	144.99	0.16	1.04×10^{-6}	0.042	6.79×10^{-9}
	^{259}Md	136.21	0.17	7.97×10^{-8}		1.32×10^{-8}
^{30}Si + ^{254}Es	^{259}Md + 1n	145.89	0.15	1.42×10^{-7}	0.031	6.76×10^{-10}
	^{260}Md	138.93	0.16	1.70×10^{-8}		2.77×10^{-9}
	^{260}Md + 1n	157.97	0.14	4.57×10^{-10}	0.109	7.10×10^{-12}
	^{261}Md	149.77	0.15	4.24×10^{-11}		6.38×10^{-12}
	^{261}Md + 1n	165.71	0.14	5.01×10^{-12}	0.064	4.37×10^{-14}
	^{258}Md	153.78	0.12	2.52×10^{-7}		3.15×10^{-8}
	^{258}Md + 1n	163.94	0.12	1.26×10^{-6}	0.042	6.23×10^{-9}
	^{259}Md	154.96	0.12	8.31×10^{-8}		1.03×10^{-8}
^{36}S + ^{254}Es	^{259}Md + 1n	164.01	0.12	2.73×10^{-7}	0.031	9.85×10^{-10}
	^{260}Md	156.89	0.12	2.89×10^{-8}		3.53×10^{-9}
	^{260}Md + 1n	168.30	0.11	5.67×10^{-8}	0.109	7.04×10^{-10}
	^{261}Md	159.92	0.12	4.36×10^{-9}		5.24×10^{-10}
	^{261}Md + 1n	170.81	0.11	4.33×10^{-9}	0.064	3.12×10^{-11}
	^{258}Md	170.93	0.10	5.17×10^{-8}		5.30×10^{-9}
	^{258}Md + 1n	181.92	0.10	1.87×10^{-7}	0.042	7.56×10^{-10}
	^{259}Md	172.83	0.10	1.13×10^{-8}		1.15×10^{-9}

TABLE I. (*Continued.*)

Reactions	Isotopes	$E_{\text{c.m.}}$ (MeV)	σ_{cap} (b)	$Y_{Z,N}$	W_{1n}	$\sigma_{Z,N}$ (b)
$^{40}\text{Ar} + ^{254}\text{Es}$	$^{259}\text{Md} + 1n$	182.38	0.10	3.31×10^{-8}	0.031	9.77×10^{-11}
	^{260}Md	175.17	0.10	3.34×10^{-9}		3.34×10^{-10}
	$^{260}\text{Md} + 1n$	187.94	0.09	3.91×10^{-9}	0.109	3.96×10^{-11}
	^{261}Md	179.44	0.10	2.92×10^{-10}		2.85×10^{-11}
	$^{261}\text{Md} + 1n$	190.59	0.09	3.30×10^{-10}	0.064	1.94×10^{-12}
	^{258}Md	192.74	0.08	4.71×10^{-5}		3.66×10^{-6}
	$^{258}\text{Md} + 1n$	203.77	0.07	7.89×10^{-5}	0.042	2.44×10^{-7}
	^{259}Md	194.42	0.08	6.67×10^{-6}		5.14×10^{-7}
$^{48}\text{Ca} + ^{254}\text{Es}$	$^{259}\text{Md} + 1n$	202.81	0.07	3.11×10^{-5}	0.031	7.08×10^{-8}
	^{260}Md	195.40	0.08	3.85×10^{-6}		2.96×10^{-7}
	$^{260}\text{Md} + 1n$	207.77	0.07	2.56×10^{-6}	0.109	2.01×10^{-8}
	^{261}Md	199.05	0.08	2.06×10^{-7}		1.56×10^{-8}
	$^{261}\text{Md} + 1n$	208.42	0.07	4.54×10^{-7}	0.064	2.09×10^{-9}
	^{258}Md	210.80	0.07	2.11×10^{-8}		1.50×10^{-9}
	$^{258}\text{Md} + 1n$	221.53	0.07	1.17×10^{-7}	0.042	3.33×10^{-10}
	^{259}Md	212.12	0.07	6.88×10^{-9}		4.86×10^{-10}
$^{50}\text{Ti} + ^{254}\text{Es}$	$^{259}\text{Md} + 1n$	222.33	0.07	1.62×10^{-8}	0.031	3.37×10^{-11}
	^{260}Md	214.88	0.07	1.60×10^{-9}		1.11×10^{-10}
	$^{260}\text{Md} + 1n$	229.02	0.07	1.10×10^{-9}	0.109	7.81×10^{-12}
	^{261}Md	220.24	0.07	7.96×10^{-11}		5.42×10^{-12}
	$^{261}\text{Md} + 1n$	231.08	0.06	1.29×10^{-10}	0.064	5.37×10^{-13}

$^{248}\text{Es} \rightarrow {}^{36\text{–}32}\text{S} + {}^{258\text{–}262}\text{Md}$, $^{48}\text{Ca} + ^{254}\text{Es} \rightarrow {}^{50}\text{Ca} + {}^{252}\text{Es} \rightarrow {}^{44\text{–}37}\text{Ar} + {}^{258\text{–}265}\text{Md}$, and $^{50}\text{Ti} + ^{254}\text{Es} \rightarrow {}^{54}\text{Ti} + {}^{250}\text{Es} \rightarrow {}^{46\text{–}41}\text{Ca} + {}^{258\text{–}263}\text{Md}$.

These schemes are used to calculate the values of $\sigma_{Z,N}$. As seen in Fig. 2, the increase of Md neutron number by one unit results in about 5 times smaller production cross section. In the $^{14}\text{C} + ^{254}\text{Es}$ reaction, the larger yield of ^{260}Md, compared to the yields of ^{258}Md and ^{259}Md, is mainly because of the Q value (smaller value of B_R^{qf}). However, in this very asymmetric reaction, the yield of ^{261}Md falls down more quickly than in the more symmetric reactions. The reactions $^{22}\text{Ne} + ^{254}\text{Es}$, $^{26}\text{Mg} + ^{254}\text{Es}$, $^{30}\text{Si} + ^{254}\text{Es}$, and $^{36}\text{S} + ^{254}\text{Es}$ are found to result in similar yields of $^{258\text{–}260}$Md but at different values of the optimal bombarding energy. For example, the values of the optimal $E_{\text{c.m.}}$ to produce ^{260}Md in the reactions $^{22}\text{Ne} + ^{254}\text{Es}$, $^{26}\text{Mg} + ^{254}\text{Es}$, $^{30}\text{Si} + ^{254}\text{Es}$, and $^{36}\text{S} + ^{254}\text{Es}$ are 101.8, 118.5, 138.9, and 156.9 MeV, respectively. Among all reactions considered, the $^{48}\text{Ca} + ^{254}\text{Es}$ reaction seems favorable to the production of presently unknown isotopes $^{261\text{–}265}$Md. The reactions of $^{14}\text{C} + ^{254}\text{Es}$ and $^{18}\text{O} + ^{254}\text{Es}$ would result in relatively larger production cross sections of the heaviest known isotopes $^{258\text{–}260}$Md. The reactions of ^{22}Ne, ^{26}Mg, and $^{30}\text{Si} + ^{254}\text{Es}$ are not in favor of producing the heaviest isotopes of Md. The use of the radioactive beams with the $Z < 16$ nuclei does not lead to the gain in the production cross section of neutron-rich Md in comparison with the ^{48}Ca-induced reactions [39].

Using the stable beam of ^{48}Ca, one can obtain neutron-rich Md isotopes in the $0n$ evaporation channel of multinucleon transfer reactions $^{48}\text{Ca} + ^{249\text{–}252}\text{Cf}$ (Fig. 3). The production cross sections for neutron-rich Md isotopes predicted in the reactions with the ^{48}Ca beam are larger than 1 pb and similar to those presented in Fig. 2. The yield of neutron-rich isotope increases by about one order of magnitude with each additional neutron in the interacting nuclei. This trend is well seen in Fig. 3 for almost all isotopes of Md. Therefore, the $^{48}\text{Ca} + ^{252}\text{Cf}$ reaction seems to be the best to produce ^{258,259,260,261,262,263,264,265}Md isotopes with the cross sections of 124 nb, 138 nb, 24 nb, 16 nb, 0.7 nb, 0.6 nb, 13 pb, and 4 pb, respectively.

If the incident energies are higher than those used in Figs. 2 and 3, the neutrons can be evaporated from the primary excited products. In this case, we need to consider one neutron ($1n$) evaporation channel. The production cross sections in $1n$ channel are calculated (Figs. 4 and 5) for the same reactions presented in Figs. 2 and 3. Note that in the production of Md isotopes, neutron evaporation strongly competes with fission and that in order to obtain the largest $\sigma_{Z,N}$ after one neutron evaporation occurs, the value of $E_{\text{c.m.}}$ must be taken at the maximum of excitation function. Taking into consideration the beam intensities, the reactions $^{48}\text{Ca} + ^{254}\text{Es}$ and $^{48}\text{Ca} + ^{251,252}$ Cf are more suitable for the production of the $^{258\text{–}264}$Md isotopes with cross sections larger than 10 pb in the $1n$ channel.

The yields of primary products increase with $E_{\text{c.m.}}$. If this increase is large enough to compensate decreasing survival probability, the cross sections in the $1n$ evaporation channel could be similar to those in the $0n$ evaporation channel. We find that the results for the $1n$ channel differ up to a few times from those for the $0n$ channel. The differences in the production cross sections between $0n$ and $1n$ channels are quite large in the reactions with ^{22}Ne, ^{26}Mg, and ^{30}Si

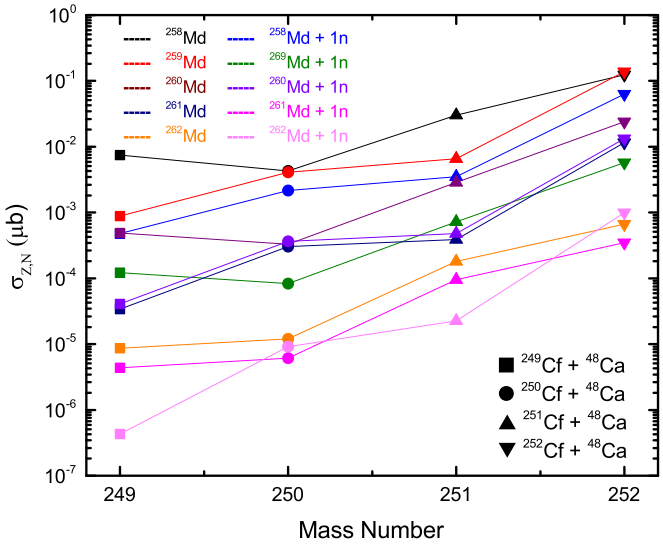

FIG. 7. The expected maximal production cross sections of $^{258–262}$Md as a function of mass number of the Cf target in the 0n and 1n evaporation channels of the indicated multinucleon transfer reactions ^{48}Ca + ^{249}Cf (squares), ^{48}Ca + ^{250}Cf (circles), ^{48}Ca + ^{251}Cf (triangles), and ^{48}Ca + ^{252}Cf (inverted triangles). The lines with different colors correspond to different isotopes of Md produced with different channels.

projectiles, but they become smaller in the reactions with ^{36}S, ^{48}Ca, and ^{50}Ti (see Fig. 6). The production of heavier isotopes occurs with close cross sections in the 0n and 1n channels of the reactions with ^{48}Ca projectile. For better understanding of the structure in Fig. 6, the values of $\sigma_{\rm cap}$ and $Y_{Z,N}$ are presented in Table I. For the 1n evaporation channels, the values of $W_{\rm sur}$ are listed as well. The production cross sections of the Md isotopes generally increase with mass number of Cf target both in the 0n and 1n channels when the reactions occur with ^{48}Ca beam (Fig. 7). According to the results in Figs. 6 and 7, the reactions ^{48}Ca + ^{254}Es and ^{48}Ca + ^{251,252} Cf seem to produce neutron-rich Md isotopes favorably.

Because of some uncertainties in the determination of neutron separation energy and fission barrier height for unknown isotopes, we study here how sensitively our calculated results change with the variation of these values. We find that reducing the values of S_n and B_f by half results in the decrease of the production cross sections of neutron-rich Md isotopes almost by a factor of 2 or 3. So, with the excitation function for production of unknown isotope in the 0n channel, one can perhaps estimate the values of S_n or B_f (if $S_n > B_f$).

IV. SUMMARY

Because the neutron-rich isotopes of Md cannot be produced in the complete fusion and fragmentation reactions due to the lack of proper projectile-target combinations, the multinucleon transfer reactions provide a unique way to produce these nuclei. The transfer reactions ^{48}Ca + ^{254}Es and ^{48}Ca + ^{251,252} Cf seem favorable to the production of the neutron-rich Md isotopes. In the comparison with our previous study [39], we find that some production cross sections are saturated as the charge number of the target increases. For heavy neutron-rich isotopes ($^{259–261}$Md), the 0n evaporation channel has larger production cross sections than the 1n evaporation channel when the projectile has the small charge number (<16), but the difference decreases for the large charge number of the projectile. We also find that lighter isotopes of Md have larger production cross sections than heavier ones in both cases of the 0n and 1n evaporation channels. However, the production of heavier isotopes occurs with close cross sections in the 0n and 1n evaporation channels. In future experiments, one can increase the target thickness if a sufficient amount of target material is available. As shown in Ref. [39] already the use of radioactive beams of nuclei with $Z < 16$ does not have any gain in the production cross sections of neutron-rich Md in comparison with the reactions involving ^{48}Ca projectile.

ACKNOWLEDGMENTS

The work of M.M. was supported by the Korea Institute of Science and Technology Information (KISTI). M.M. and K.K. are also partly supported by Basic Science Research Program through the National Research Foundation of Korea (Grant No. 2016R1A5A1013277). This work was also supported by RFBR (No. 17-52-12015 and No. 17-52-45037) and DFG. The work of N.V.A. was supported by Tomsk Polytechnic University Competitiveness Enhancement Program grant.

[1] V. V. Volkov, Phys. Rep. **44**, 93 (1978).
[2] V. V. Volkov, in *Treatise on Heavy-Ion Science*, edited by D. A. Bromley (Plenum Press, New York, 1989), Vol. 8, Chap. 2, pp. 101–203.
[3] W. U. Schröder and J. R. Huizenga, in *Treatise on Heavy-Ion Science*, edited by D. A. Bromley (Plenum Press, New York, 1985), Vol. 2, pp. 113–726.
[4] M. Schädel, W. Brüchle, H. Gäggeler, J. V. Kratz, K. Sümmerer, G. Wirth, G. Herrmann, R. Stakemann, G. Tittel, N. Trautmanna *et al.*, Phys. Rev. Lett. **48**, 852 (1982).
[5] H. H. Freiesleben and J. V. Kratz, Phys. Rep. **106**, 1 (1984).
[6] H. Gäggeler, W. Brüchle, M. Brügger *et al.*, Phys. Rev. C **33**, 1983 (1986).
[7] C. Y. Wu, X. T. Liu, S. P. Sorensen, R. W. Kincaid, M. W. Guidry, D. Cline, W. J. Kernan, E. Vogt, T. Czosnyka, A. E. Kavka *et al.*, Phys. Lett. B **188**, 25 (1987).
[8] C. Y. Wu, W. von Oertzen, D. Cline, and M. W. Guidry, Ann. Rev. Nucl. Part. Sci. **40**, 285 (1990).
[9] R. Broda, M. A. Quader, P. J. Daly, R. V. F. Janssens, T. L. Khoo, W. Ma, and M. W. Drigert, Phys. Lett. B **251**, 245 (1990).
[10] A. Türler, H. R. von Gunten, J. D. Leyba *et al.*, Phys. Rev. C **46**, 1364 (1992).
[11] G. G. Adamian, A. K. Nasirov, N. V. Antonenko, and R. V. Jolos, Phys. Part. Nucl. **25**, 583 (1994).

[12] W. von Oertzen and A. Vitturi, Rep. Prog. Phys. **64**, 1247 (2001).
[13] B. Fornal, S. Zhu, R. V. F. Janssens *et al.*, Phys. Rev. C **70**, 064304 (2004).
[14] M. Rejmund, S. Bhattacharyya, A. Navin, W. Mittig, L. Gaudefroy, M. Gelin, G. Mukherjee, F. Rejmund, P. Roussel-Chomaz, and C. Theisen, Phys. Rev. C **76**, 021304(R) (2007).
[15] L. Corradi, G. Pollarolo, and S. Szilner, J. Phys. G **36**, 113101 (2009).
[16] S. Lunardi, in *Perspective in Nuclear Physics: Proceedings of the 6th Japan–Italy Symposium on Heavy–Ion Physics*, AIP Conf. Proc. No. 1120 (AIP, New York, 2009), p. 70.
[17] W. Królas, R. Broda, B. Fornal, T. Pawłat, J. Wrzesiński, D. Bazzacco, G. de Angelis, S. Lunardi, R. Menegazzo, D. R. Napoli, and C. Rossi Alvarez, Nucl. Phys. A **832**, 170 (2010).
[18] S. Heinz, V. Comas, S. Hofmann, D. Ackermann, J. Heredia, F. P. Hessberger, J. Khuyagbaatar, B. Kindler, B. Lommel, and R. Mann, Eur. Phys. J. A **43**, 181 (2010).
[19] W. Loveland, A. M. Vinodkumar, D. Peterson, and J. P. Greene, Phys. Rev. C **83**, 044610 (2011).
[20] S. A. Kalandarov, G. G. Adamian, and N. V. Antonenko, Phys. Part. Nuclei **43**, 825 (2012).
[21] V. Comas, S. Heinz, S. Hofmann, D. Ackermann, J. Heredia, F. P. Hessberger, J. Khuyagbaatar, B. Kindler, B. Lommel, and R. Mann, Eur. Phys. J. A **48**, 180 (2012).
[22] V. F. Comas, S. Heinz, S. Hofmann, D. Ackermann, J. Heredia, F. P. Hessberger, J. Khuyagbaatar, B. Kindler, B. Lommel, and R. Mann, Eur. Phys. J. A **49**, 112 (2013).
[23] E. M. Kozulin, G. N. Knyazheva, S. N. Dmitriev *et al.*, Phys. Rev. C **89**, 014614 (2014).
[24] H. M. Devaraja, S. Heinz, O. Belushkina *et al.*, Phys. Lett. B **748**, 199 (2015).
[25] S. Heinz, H. M. Devaraja, O. Belushkina *et al.*, Eur. Phys. J. A **52**, 278 (2016).
[26] I. Stefan, B. Fornal, S. Leoni *et al.*, Phys. Lett. B **779**, 456 (2018).
[27] W. Reisdorf, J. V. Kratz, R. Bellwied *et al.*, Z. Phys. A **342**, 411 (1992).
[28] G. A. Souliotis, M. Veselsky, G. Chubarian *et al.*, Phys. Lett. B **543**, 163 (2002).
[29] V. Jha, B. J. Roy, A. Chatterjee, and H. Machner, Eur. Phys. J. A **19**, 347 (2004).
[30] Y. X. Watanabe, Y. H. Kim, S. C. Jeong, Y. Hirayama, N. Imai, H. Ishiyama, H. S. Jung, H. Miyatake, S. Choi, J. S. Song *et al.*, Phys. Rev. Lett. **115**, 172503 (2015).
[31] N. Wang and L. Guo, Phys. Lett. B **760**, 236 (2016).
[32] T. Mijatovic, S. Szilner, L. Corradi *et al.*, Phys. Rev. C **94**, 064616 (2016).
[33] T. Welsh, W. Loveland, R. Yanez *et al.*, Phys. Lett. B **771**, 119 (2017).
[34] A. Di Nitto, J. Khuyagbaatar, D. Ackermann *et al.*, Phys. Lett. B **784**, 199 (2018).
[35] Y. E. Penionzhkevich, G. G. Adamian, and N. V. Antonenko, Phys. Lett. B **621**, 119 (2005).
[36] Y. E. Penionzhkevich, G. G. Adamian, and N. V. Antonenko, Eur. Phys. J. A **27**, 187 (2006).
[37] M.-H. Mun, G. G. Adamian, N. V. Antonenko, Y. Oh, and Y. Kim, Phys. Rev. C **89**, 034622 (2014).
[38] M.-H. Mun, G. G. Adamian, N. V. Antonenko, Y. Oh, and Y. Kim, Phys. Rev. C **91**, 054610 (2015).
[39] M.-H. Mun, G. G. Adamian, N. V. Antonenko, and Y.-O. Lee, Eur. Phys. J. **52**, 363 (2016).
[40] N. V. Antonenko, E. A. Cherepanov, A. K. Nasirov, V. P. Permjakov, and V. V. Volkov, Phys. Lett. B **319**, 425 (1993).
[41] N. V. Antonenko, E. A. Cherepanov, A. K. Nasirov, V. P. Permjakov, and V. V. Volkov, Phys. Rev. C **51**, 2635 (1995).
[42] G. G. Adamian, N. V. Antonenko, and W. Scheid, Nucl. Phys. A **618**, 176 (1997); G. G. Adamian, N. V. Antonenko, W. Scheid, and V. V. Volkov, *ibid.* **627**, 361 (1997); **633**, 409 (1998).
[43] G. G. Adamian, N. V. Antonenko, R. V. Jolos, S. P. Ivanova, and O. I. Melnikova, Int. J. Mod. Phys. E **5**, 191 (1996).
[44] W. D. Myers and W. J. Swiatecki, Phys. Rev. C **62**, 044610 (2000).
[45] J. Hong, G. G. Adamian, and N. V. Antonenko, Phys. Rev. C **94**, 044606 (2016).
[46] P. Möller, J. R. Nix, T. Ichikawa, and H. Sagawa, At. Data Nucl. Data Tables **109–110**, 1 (2016); P. Möller, A. J. Sierk, T. Ichikawa, A. Iwamoto, R. Bengtsson, H. Uhrenholt, and S. Åberg, Phys. Rev. C **79**, 064304 (2009).
[47] Y. Ito, P. Schury, M. Wada *et al.*, Phys. Rev. Lett. **120**, 152501 (2018).
[48] N. Wang, M. Liu, X. Wu, and J. Meng, Phys. Lett. B **734**, 215 (2014); www.imqmd.com/mass/